NASA Technical Memorandum 89120

UNSTEADY TRANSONIC FLOW CALCULATIONS FOR REALISTIC AIRCRAFT CONFIGURATIONS

JOHN T. BATINA
DAVID A. SEIDEL
SAMUEL R. BLAND
ROBERT M. BENNETT

MARCH 1987

National Aeronautics and
Space Administration

Langley Research Center
Hampton, Virginia 23665

UNSTEADY TRANSONIC FLOW CALCULATIONS FOR REALISTIC AIRCRAFT CONFIGURATIONS

John T. Batina, David A. Seidel, Samuel R. Bland, and Robert M. Bennett
NASA Langley Research Center
Hampton, Virginia 23665-5225

Abstract

A transonic unsteady aerodynamic and aeroelasticity code has been developed for application to realistic aircraft configurations. The new code is called CAP-TSD which is an acronym for Computational Aeroelasticity Program - Transonic Small Disturbance. The CAP-TSD code uses a time-accurate approximate factorization (AF) algorithm for solution of the unsteady transonic small-disturbance equation. The AF algorithm is very efficient for solution of steady and unsteady transonic flow problems. It can provide accurate solutions in only several hundred time steps yielding a significant computational cost savings when compared to alternative methods. The new code can treat complete aircraft geometries with multiple lifting surfaces and bodies including canard, wing, tail, control surfaces, launchers, pylons, fuselage, stores, and nacelles. Applications are presented for a series of five configurations of increasing complexity to demonstrate the wide range of geometrical applicability of CAP-TSD. These results are in good agreement with available experimental steady and unsteady pressure data. Calculations for the General Dynamics one-ninth scale F-16C aircraft model are presented to demonstrate application to a realistic configuration. Unsteady results for the entire F-16C aircraft undergoing a rigid pitching motion illustrated the capability required to perform transonic unsteady aerodynamic and aeroelastic analyses for such configurations.

Nomenclature

c	airfoil chord
c_r	wing reference chord
C_a	body angle-of-attack correction
C_p	pressure coefficient
C_p	unsteady pressure coefficient normalized by oscillation amplitude
C_t	body thickness correction
f	function defining position of horizontal lifting surface
g	function defining position of vertical lifting surface
k	reduced frequency, $\omega c_r/2U$
M	freestream Mach number
$N(x,y,z,t)$	function defining body surface
t	time, nondimensionalized by U/c_r
U	freestream velocity
α	angle of attack
β	yaw angle
γ	ratio of specific heats
δ	control surface deflection angle
$\Delta\tilde{C}_p$	unsteady lifting pressure coefficient normalized by oscillation amplitude
Δt	nondimensional time step
$\bar{\eta}$	fractional semispan along exposed planform
θ	polar angle of body cross-section defined in Figs. 7 and 12
Λ	leading edge sweep angle
ϕ	disturbance velocity potential
ω	angular frequency

Subscripts

b	body
c	canard
f	fuselage
t	tail
w	wing
0	mean value
1	dynamic value

Introduction

Presently, considerable research is being conducted to develop finite-difference computer codes for calculating transonic unsteady aerodynamics for aeroelastic applications.[1] These computer codes are being developed to provide accurate methods of calculating unsteady airloads for the prediction of aeroelastic phenomena such as flutter and divergence. For example, the XTRAN3S[2] unsteady transonic small-disturbance (TSD) code was developed for transonic aeroelastic analyses of isolated planar wings. The code uses an alternating-direction implicit (ADI) finite-difference algorithm to calculate steady and unsteady transonic flows in a time-marching fashion. Several terms of the ADI algorithm are treated explicitly, though, which leads to a time step restriction based on numerical stability considerations. Experience with the code has shown that for applications to practical wings with moderate to high sweep and taper, very small time steps are required for the algorithm to be numerically stable.[3-6] This stability restriction typically results in thousands of time steps required to obtain converged steady solutions and thousands of steps per cycle of

motion. Such solutions are computationally expensive, and thus, aeroelastic applications of XTRAN3S have generally been limited.

A new alternative algorithm based on approximate factorization (AF) was recently developed by Batina[7] for the time-accurate solution of the unsteady TSD equation. The AF algorithm involves a Newton linearization procedure coupled with an internal iteration technique. In Ref. 7 the AF algorithm was shown to be very robust and efficient for application to either steady or oscillatory transonic flows with subsonic or supersonic freestream conditions. The new algorithm can provide accurate solutions in only several hundred time steps yielding a significant computational cost savings when compared to alternative methods. Furthermore, the AF algorithm is fully vectorizable which results in an additional saving of computer resources. The Unsteady Aerodynamics Branch at NASA Langley Research Center has subsequently developed a new computer code to fully exploit the superior stability characteristics and computational efficiency of the AF algorithm. The new code is called CAP-TSD which is an acronym for Computational Aeroelasticity Program - Transonic Small Disturbance. The code allows the analysis of complete aircraft configurations including fuselages and multiple lifting surfaces. The development of the methodology for treating these components has been reported in Refs. 8 and 9. The CAP-TSD code also can treat pylons, stores, and nacelles using modeling similar to that of Boppe and Stern[10] and Shankar and Malmuth.[11] The CAP-TSD code therefore is capable of transonic unsteady aerodynamic and aeroelastic analysis of realistic aircraft configurations.

The purpose of this paper is to describe the development of the CAP-TSD computer code and to present unsteady transonic applications for realistic aircraft configurations involving multiple components. Specifically, the paper will: (1) state the governing flow field equations, (2) briefly reiterate the AF algorithm and solution procedure, (3) discuss the computational modeling of the wing, canard, tail, fuselage, pylons, stores, and nacelles in the context of the unsteady TSD equation, (4) introduce the CAP-TSD computer code, and (5) present results for several complex configurations which demonstrate the wide range of geometrical applicability of the new code. Finally, the results are validated by making comparisons with available experimental steady and unsteady data.

Governing Equations

In this section, the TSD equation, boundary conditions, and coordinate transformation are briefly described.

TSD Equation

The flow is assumed to be governed by the general frequency modified TSD potential equation which may be written in conservation law form as

$$\frac{\partial f_0}{\partial t} + \frac{\partial f_1}{\partial x} + \frac{\partial f_2}{\partial y} + \frac{\partial f_3}{\partial z} = 0 \tag{1}$$

where

$$f_0 = - A\phi_t - B\phi_x \tag{2a}$$

$$f_1 = E\phi_x + F\phi_x^2 + G\phi_y^2 \tag{2b}$$

$$f_2 = \phi_y + H\phi_x\phi_y \tag{2c}$$

$$f_3 = \phi_z \tag{2d}$$

The coefficients A, B, and E are defined as

$$A = M^2, \; B = 2M^2, \; E = 1 - M^2 \tag{3}$$

Several choices are available for the coefficients F, G, and H depending upon the assumptions used in deriving the TSD equation.[2] Briefly, the coefficients are referred to as "NASA Ames" coefficients when defined as

$$F = - \frac{1}{2} (\gamma + 1) M^2 \tag{4a}$$

$$G = \frac{1}{2} (\gamma - 3) M^2 \tag{4b}$$

$$H = - (\gamma - 1) M^2 \tag{4c}$$

and are referred to as "NLR" coefficients when defined as

$$F = - \frac{1}{2} [3 - (2 - \gamma)M^2]M^2 \tag{5a}$$

$$G = - \frac{1}{2} M^2 \tag{5b}$$

$$H = - M^2 \tag{5c}$$

The "classical" coefficients are given by

$$F = - \frac{1}{2} (\gamma + 1) M^2 \tag{6a}$$

$$G = 0 \tag{6b}$$

$$H = 0 \tag{6c}$$

and finally the coefficients for the linear equation are

$$F = G = H = 0 \tag{7}$$

Boundary Conditions

The conditions imposed upon the outer boundary of the computational region are similar to the characteristic or "nonreflecting" boundary conditions reported by Whitlow.[12] The conditions employed here are given by

Upstream: $$\phi = 0 \qquad (8a)$$

Downstream: $$\frac{1}{2}\left(\frac{-B}{C} + \frac{D}{\sqrt{C}}\right)\phi_t + \phi_x = 0 \qquad (8b)$$

Above: $$\frac{D}{2}\phi_t + \phi_z = 0 \qquad (8c)$$

Below: $$\frac{D}{2}\phi_t - \phi_z = 0 \qquad (8d)$$

Right spanwise: $$\frac{D}{2}\phi_t + \phi_y = 0 \qquad (8e)$$

Left spanwise: $$\frac{D}{2}\phi_t - \phi_y = 0 \qquad (8f)$$

(for full-span modeling)

Symmetry plane: $$\phi_y = 0 \qquad (8g)$$

(for half-span modeling)

where $C = E + 2F\phi_x$ and $D = \sqrt{4A + B^2/C}$. Note that when marching to steady-state, the time derivatives in Eqs. (8b) to (8f) vanish resulting in simple Neumann boundary conditions.

The horizontal lifting surfaces (canard/wing/horizontal tail/launcher) are modeled by imposing the following boundary conditions:

Flow tangency: $$\phi_z^{\pm} = f_x^{\pm} + f_t \qquad (9a)$$

Trailing wake: $$[\phi_z] = 0 \qquad (9b)$$

$$[\phi_x + \phi_t] = 0 \qquad (9c)$$

where [ ] indicates the jump in the indicated quantity across the wake. The flow-tangency condition is imposed along the mean plane of the respective lifting surface. In Eq. (9a), the plus and minus superscripts indicate the upper and lower surfaces of the mean plane, respectively. The wakes are assumed to be flat and horizontal. The numerical implementation of Eqs. (9) allows for coplanar as well as non-coplanar combinations of canard, wing, horizontal tail, and launchers.

The vertical lifting surfaces (pylon/vertical tail) are modeled by imposing the following boundary conditions:

Flow tangency: $$\phi_y^{\pm} = g_x^{\pm} + g_t \qquad (10a)$$

Trailing wake: $$[\phi_y] = 0 \qquad (10b)$$

$$[\phi_x + \phi_t] = 0 \qquad (10c)$$

where [ ] again indicates the jump in the indicated quantity across the wake. The flow-tangency condition is imposed along the vertical (x-z) mean plane of the respective lifting surface. In Eq. (10a), the plus and minus superscripts indicate the right and left surfaces of the mean plane, respectively. Flat vertical wakes are assumed for the pylons and vertical tail.

Bodies such as the fuselage, stores, and nacelles are treated as follows. For a body at angle of attack α_b and at yaw angle β_b, the exact flow-tangency boundary condition may be written as

$$N_t + N_x(1 + \phi_x) + N_y(\phi_y + \beta_b) + N_z(\phi_z + \alpha_b) = 0 \qquad (11)$$

where $N(x,y,z,t) = 0$ defines the body surface. Computationally, bodies are modeled by applying simplified boundary conditions on a prismatic surface rather than on the true surface.[10,11] The method is consistent with the small-disturbance approximation and treats bodies with sufficient accuracy to obtain the correct global effect on the flow field without the use of special grids or complicated coordinate transformations. As such, the approximations to the flow-tangency boundary condition (Eq. 11) imposed on the prismatic surface are

Upstream face: $$\phi_x = V_{inlet} - 1 \qquad (12a)$$

Downstream face: $$\phi_x = V_{exit} - 1 \qquad (12b)$$

Left/right faces: $$\phi_y = -C_t\left(\frac{N_x}{N_y} + \frac{N_t}{N_y}\right) - C_a\beta_b \qquad (12c)$$

Top/bottom faces: $$\phi_z = -C_t\left(\frac{N_x}{N_z} + \frac{N_t}{N_z}\right) - C_a\alpha_b \qquad (12d)$$

where V_{inlet} and V_{exit} are inlet and exit flow velocities, respectively, specified in the case of a nacelle as derived in Ref. 10. The parameters C_t and C_a are thickness and angle-of-attack corrections, respectively, derived using slender body theory to account for the spatial differences between true and prismatic body surfaces.

The simplified body boundary conditions (Eqs. (12)) are analogous to the lifting surface flow-tangency boundary conditions which are imposed on the mean plane of the lifting surface rather than on the true surface. This method has been shown to be accurate for steady transonic applications for configurations with a fuselage, stores, and flow-through nacelles.[10] The body boundary conditions presented herein are extensions of those reported in Ref. 10, to allow analysis of unsteady transonic cases. Unsteady calculations for a wing/fuselage

configuration were reported in Ref. 9, using body modeling similar to Eqs. (12c) and (12d).

Coordinate Transformation

The finite-difference grids in both the physical and computational domains are contained within rectangular boundaries and conform to the leading and trailing edges of the horizontal lifting surfaces. Regions in the physical domain are mapped into rectangular regions in the computational domain using the shearing transformation

$$\xi = \xi(x,y), \quad \eta = y, \quad \zeta = z \tag{13}$$

where ξ, η, and ζ are the nondimensional computational coordinates in the x, y, and z directions, respectively. For simplicity, no shearing is performed in the vertical direction so that pylons and vertical tails are approximated by rectangular surfaces.

Approximate Factorization Algorithm

An approximate factorization algorithm was developed[7] to solve the modified TSD equation (Eq. (1)) and associated boundary conditions (Eqs. (8) - (10) and (12)). In this section, the AF algorithm is briefly described.

General Description

The AF algorithm consists of a Newton linearization procedure coupled with an internal iteration technique. For unsteady flow calculations, the solution procedure involves two steps. First, a time linearization step (described below) is performed to determine an estimate of the potential field. Second, internal iterations are performed to provide time accurate modeling of the flow field. Specifically, the TSD equation (Eq. (1)) is written in general form as

$$R(\phi^{n+1}) = 0 \tag{14}$$

where ϕ^{n+1} represents the unknown potential field at time level (n+1). The solution to Eq. (14) is then given by the Newton linearization of Eq. (14) about ϕ^*

$$R(\phi^*) + \left(\frac{\partial R}{\partial \phi}\right)_{\phi=\phi^*} \Delta\phi = 0 \tag{15}$$

In Eq. (15), ϕ^* is the currently available value of ϕ^{n+1} and $\Delta\phi = \phi^{n+1} - \phi^*$. During convergence of the iteration procedure, $\Delta\phi$ will approach zero so that the solution will be given by $\phi^{n+1} = \phi^*$. In general, only one or two iterations are required to achieve acceptable convergence. For steady flow calculations, iterations are not used since time accuracy is not necessary when marching to steady-state.

Mathematical Formulation

The AF algorithm is formulated by first approximating the time derivative terms (ϕ_{tt} and ϕ_{xt} terms) by second-order accurate finite-difference formulae. The TSD equation is rewritten by substituting $\phi = \phi^* + \Delta\phi$ and neglecting squares of derivatives of $\Delta\phi$ which is equivalent to applying Eq. (15) term by term. The resulting equation is then rearranged and the left-hand side is approximately factored into a triple product of operators yielding

$$L_\xi L_\eta L_\zeta \Delta\phi = -R(\phi^*, \phi^n, \phi^{n-1}, \phi^{n-2}) \tag{16}$$

where

$$L_\xi = 1 + \frac{3B}{4A}\xi_x \Delta t \frac{\partial}{\partial\xi} - \xi_x \frac{\Delta t^2}{2A}\frac{\partial}{\partial\xi} F_1 \frac{\partial}{\partial\xi} \tag{17a}$$

$$L_\eta = 1 - \xi_x \frac{\Delta t^2}{2A}\frac{\partial}{\partial\eta} F_2 \frac{\partial}{\partial\eta} \tag{17b}$$

$$L_\zeta = 1 - \xi_x \frac{\Delta t^2}{2A}\frac{\partial}{\partial\zeta} F_3 \frac{\partial}{\partial\zeta} \tag{17c}$$

$$F_1 = E\xi_x + 2F\xi_x^2\phi_\xi^* + 2G\xi_y(\xi_y\phi_\xi^* + \phi_\eta^*) + \frac{\xi_y^2}{\xi_x}(1 + H\xi_x\phi_\xi^*) + H\xi_y(\xi_y\phi_\xi^* + \phi_\eta^*) \tag{17d}$$

$$F_2 = \frac{1}{\xi_x}(1 + H\xi_x\phi_\xi^*) \tag{17e}$$

$$F_3 = \frac{1}{\xi_x} \tag{17f}$$

$$R = -\xi_x \frac{\Delta t^2}{2A}\left\{ -\frac{A}{\xi_x}\frac{2\phi^* - 5\phi^n + 4\phi^{n-1} - \phi^{n-2}}{\Delta t^2} - B\frac{3\phi_\xi^* - 4\phi_\xi^n + \phi_\xi^{n-1}}{2\Delta t} + \frac{\partial}{\partial\xi}\left[E\xi_x\phi_\xi^* + F\xi_x^2\phi_\xi^{*2} + G(\xi_y\phi_\xi^* + \phi_\eta^*)^2 + \frac{\xi_y}{\xi_x}(\xi_y\phi_\xi^* + \phi_\eta^*) + H\xi_y\phi_\xi^*(\xi_y\phi_\xi^* + \phi_\eta^*)\right] + \frac{\partial}{\partial\eta}\left[\frac{1}{\xi_x}(\xi_y\phi_\xi^* + \phi_\eta^*) + H\phi_\xi^*(\xi_y\phi_\xi^* + \phi_\eta^*)\right] + \frac{\partial}{\partial\zeta}\left[\frac{1}{\xi_x}\phi_\zeta^*\right]\right\} \tag{17g}$$

Equation (16) is solved using three sweeps through the grid by sequentially applying the operators L_ξ, L_η, and L_ζ as

$$\xi \text{ - sweep: } L_\xi \, \Delta\bar{\phi} = - R \qquad (18a)$$

$$\eta \text{ - sweep: } L_\eta \, \Delta\bar{\bar{\phi}} = \Delta\bar{\phi} \qquad (18b)$$

$$\zeta \text{ - sweep: } L_\zeta \, \Delta\phi = \Delta\bar{\bar{\phi}} \qquad (18c)$$

For steady flow calculations, the time-derivatives of the AF algorithm are implemented for variable time stepping to allow step-size cycling for convergence acceleration. In these calculations the step size is cycled using a standard geometric sequence. Further details of the algorithm development and solution procedure may be found in Ref. 7.

Time-Linearization Step

An initial estimate of the potentials at time level (n+1) is required to start the iteration process. This estimate is provided by performing a time-linearization calculation. The equations governing the time-linearization step are derived in a similar fashion as the equations for iteration. The only difference is that the equations are formulated by linearizing about time level (n) rather than the iterate level (*). So by substituting $\phi = \phi^n + \Delta\phi$ into the TSD equation (Eq. (1)) and neglecting squares of derivatives of $\Delta\phi$, the time-linearization step may be written as

$$L_\xi \, L_\eta \, L_\zeta \, \Delta\phi = - R(\phi^n, \phi^{n-1}, \phi^{n-2}) \qquad (19)$$

where the operators L_ξ, L_η, and L_ζ are similar to those of Eq. (17) with ϕ^* replaced by ϕ^n.

Boundary Conditions

The boundary conditions are numerically imposed by redefining the L_ξ, L_η, and L_ζ operators in Eq. (16) as well as the right-hand side R, at the appropriate grid points. The equation to be solved at boundary grid points may then be written symbolically as

$$\tilde{L}_\xi \, \tilde{L}_\eta \, \tilde{L}_\zeta \, \Delta\phi = - \tilde{R} \qquad (20)$$

where the "tilde" indicates that the quantity has been modified or rewritten to account for the boundary conditions. Further details on the implementation of the boundary conditions are given in Ref. 7.

For supersonic freestream conditions, the AF algorithm is applied without modification. It is recognized, however, that the grid is not optimal for supersonic applications.

CAP-TSD Code

The AF algorithm has been used as the basis of the CAP-TSD code for transonic unsteady aerodynamic and aeroelastic analysis of realistic aircraft configurations. The present capability has the option of half-span modeling (Eq. (8g)) for symmetric cases or full-span modeling (Eq. (8f)) to allow the treatment of antisymmetric mode shapes, fuselage yaw, or unsymmetric configurations such as an oblique wing or asymmetric wing stores.

To investigate the speed and efficiency of CAP-TSD, steady and unsteady calculations were performed using an early wing-alone version of the code for the F-5 wing.[13] The freestream Mach number was 0.9 and the mean angle of attack was 0°. In these calculations, XTRAN3S[2] results were used as a standard for comparison. For the steady-state case, the XTRAN3S results were obtained using a constant step size of Δt = 0.01, which was determined by a numerical stability analysis in Ref. 7. It is also the same step size as that reported in Refs. 3 and 4. These calculations were performed for a total of 4000 time steps. The CAP-TSD results were obtained by cycling the step size through a range of values between Δt = 0.05 and 5.0. A total of 250 time steps were run. A comparison of steady-state convergence between the two codes is shown in Fig. 1. The "error" plotted in the figure is the ratio of the maximum $|\Delta\phi|$ after n time steps to the maximum $|\Delta\phi|$ in the initial solution (first time step). After 4000 steps, the error in the XTRAN3S solution was reduced by slightly greater than three orders of magnitude. The error in the CAP-TSD solution, however, was reduced by more than four orders of magnitude in only 250 steps.

To further test the stability characteristics of the CAP-TSD AF algorithm, a much more challenging case was considered. In this example, the leading edge sweep of the F-5 wing was increased to 60° by shearing the F-5 planform aft. The freestream Mach number was again selected as M = 0.9 and the mean angle of attack was 0°. The XTRAN3S results were obtained using a constant step size of Δt = 0.002, which was determined by a numerical stability analysis,[7] and the CAP-TSD results were obtained by cycling the step size through a range of values between Δt = 0.05 and 0.5. A comparison of the steady-state convergence histories between the two codes is shown in Fig. 2. The XTRAN3S solution converges very slowly such that after 4000 steps, the error has been reduced by only approximately one order of magnitude. The CAP-TSD solution, however, has converged just as rapidly as in the first example, with the error reduced over four orders of magnitude in only 250 steps.

Further computational efficiency is achieved through extensive vectorization of the AF algorithm as well as the CAP-TSD code in general. Since the L_ξ, L_η, and L_ζ operators of the AF algorithm only contain derivatives in their respective coordinate directions, all three sweeps of the solution procedure are vectorizable. This is in contrast with the alternating direction implicit algorithm of XTRAN3S which can only be

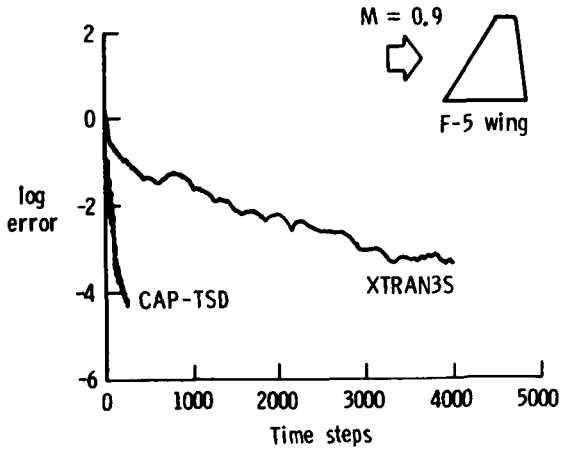

Fig. 1 Comparison of steady-state convergence between CAP-TSD and XTRAN3S for the F-5 wing at M = 0.9 and α_0 = 0°.

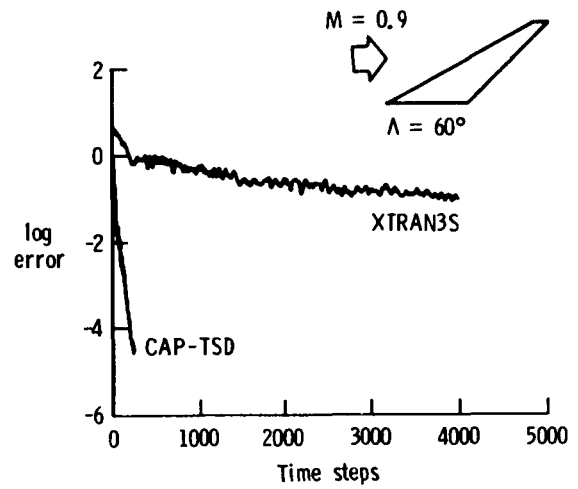

Fig. 2 Comparison of steady-state convergence between CAP-TSD and XTRAN3S for the F-5 wing sheared to Λ = 60° at M = 0.9 and α_0 = 0°.

vectorized in the streamwise direction. To quantify the computational efficiency achieved through vectorization, timing information was compared for the cases presented in Figs. 1 and 2. The vectorized XTRAN3S (Version 1.5) code required 0.62 CPU seconds per time step on the CDC VPS-32 computer at NASA Langley Research Center. For the same problem, the CAP-TSD code required only 0.10 CPU seconds per time step. Multiplying this efficiency factor of approximately six, times the factor of approximately twenty achieved through improved stability, yields a two order of magnitude decrease in computational expense using CAP-TSD for this case.

For unsteady calculations with CAP-TSD, the step size is selected based on accuracy rather than on numerical stability considerations. Consequently, a convergence study was performed in Ref. 7, using the AF algorithm, to determine the largest step size (fewest number of steps per cycle of motion) that produces converged solutions for the F-5 wing at M = 0.9. The wing was forced to oscillate in a rigid pitching motion at a reduced frequency of k = 0.137. Unsteady results were obtained for 100, 200, 300, and 400 steps per cycle of motion which required Δt = 0.2293, 0.1147, 0.0764, and 0.0573, respectively. In Ref. 7 these calculations indicated that approximately 300 steps per cycle were required to obtain converged results, although 200 steps per cycle may be acceptable for engineering purposes. Therefore, the CAP-TSD code is efficient for unsteady as well as steady transonic applications.

Results and Discussion

In this section, results are presented for a series of realistic aircraft configurations which demonstrate the efficiency, accuracy, and applicability of the CAP-TSD code. These configurations are described first, followed by a discussion of the corresponding calculations. All of the calculations were performed using the NASA Ames coefficients (Eqs. (4)) in the TSD equation and the time derivatives in the farfield boundary conditions (Eqs. (8)) were neglected in this initial application study. The results are validated by making detailed comparisons with available steady and unsteady experimental pressure data. Further applications of CAP-TSD including comparisons with experiment for supersonic freestream cases are reported by Bennett, et al.[14]

Configurations

Results are presented for the five configurations shown in Fig. 3. These configurations range in geometrical complexity from a simple wing with control surface to a realistic fighter geometry. The five configurations were selected to assess various geometry capabilities of CAP-TSD by making comparisons with the experimental pressure data of Refs. 15-21. A detailed description of each configuration is given in the following paragraphs.

The first configuration (Fig. 3(a)) is the F-5 wing with an inboard trailing edge control surface.[15] The wing has a panel aspect ratio of 1.58, a leading edge sweep angle of 31.9°, and a taper ratio of 0.28. The airfoil section of the F-5 wing is a modified NACA 65A004.8 airfoil which has a drooped nose and is symmetric aft of 40% chord. The control surface has a constant-percent-chord hinge line at 82% chord, inboard side edge at the wing root, and outboard side edge at 58% semispan. The calculations are compared with the experimental oscillatory pressure data from an F-5 wing model tested by Persoon, Roos, and Schippers.[15] Both subsonic and supersonic freestream cases are presented.

The second configuration (Fig. 3(b)) is the F-5 wing/tiptank/pylon/store geometry.[16] For

(a) F-5 wing/control surface.

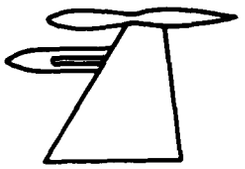

(b) F-5 wing/tiptank/pylon/store.

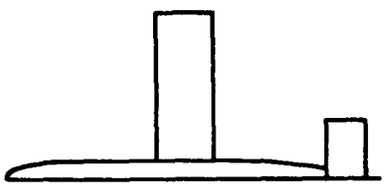

(c) DFVLR wing/fuselage/tail.

(d) Rockwell canard/wing/fuselage.

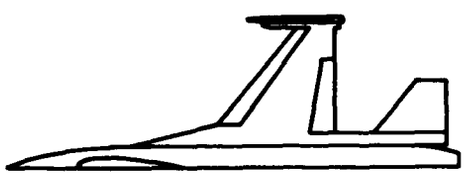

(e) General Dynamics F-16C aircraft model.

Fig. 3 Configurations for CAP-TSD analysis.

this configuration, three components have been modeled in addition to the F-5 wing: (1) an area-ruled tiptank which is an axisymmetric body of revolution with a fineness ratio (length/maximum diameter) of 10.88; (2) an underwing store which is also an axisymmetric body of revolution with a fineness ratio of 7.04; and (3) a pylon which connects the store to the lower surface of the wing at 77% semispan. The tiptank and store have angles of incidence relative to the wing zero angle of attack of -2.0° and -2.5°, respectively. A more detailed description of the F-5 wing/tiptank/pylon/store configuration is given in Refs. 16 and 17 along with the experimental pressure data. The calculations were performed for several combinations of F-5 components to investigate aerodynamic interference effects on steady and unsteady wing pressures.

For the first two configurations (Figs. 3(a) and 3(b)), unsteady as well as steady experimental pressure data are available for comparison with the CAP-TSD calculations. For the remaining configurations, however, only steady experimental pressure data exist to assess the accuracy of the calculated results.

The third configuration (Fig. 3(c)) is a simple wing/fuselage/tail model that was tested at the DFVLR.[18] The model consists of a rectangular-planform wing that is centrally mounted to a circular cross-section fuselage with a T-tail. The wing has a panel (exposed) aspect ratio of 2.66 and an RAE 101 airfoil section (9% maximum thickness-to-chord ratio). The axisymmetric fuselage has a fineness ratio of 9.75. The horizontal tail has a panel aspect ratio of 1.5 and an RAE 101 airfoil section (12.7% maximum thickness-to-chord ratio). It is located above the wing mean plane, a distance equal to the fuselage maximum diameter, and is connected to the fuselage by the rectangular vertical tail. The DFVLR wing/fuselage/tail configuration is further described in Ref. 18 along with the low-speed experimental steady pressure data.

The fourth configuration (Fig. 3(d)) is a canard/wing/fuselage model that was tested by Rockwell International.[19] The model consists of a swept-tapered canard and wing mounted to a relatively simple half-span fuselage. Each of the non-coplanar lifting surfaces has a panel (exposed) aspect ratio of approximately 1.0, a leading edge sweep angle of 40°, a taper ratio slightly greater than 0.25, and a supercritical airfoil section. The wing also has 4° of incidence relative to the fuselage and 5° of parabolic twist washout. The Rockwell canard/wing/fuselage configuration is further described in Ref. 19 along with the experimental steady pressure data.

The fifth configuration (Fig. 3(e)) is the one-ninth scale F-16C aircraft model that was tested by General Dynamics.[20] Shown in Fig. 4 are the F-16C components that are modeled using CAP-TSD. The F-16C is modeled using four lifting surfaces and two bodies. The lifting surfaces include: (1) the wing with leading and trailing edge control surfaces, (2) the launcher, (3) a highly-swept strake, aft strake, and shelf surface, and (4) the horizontal tail.

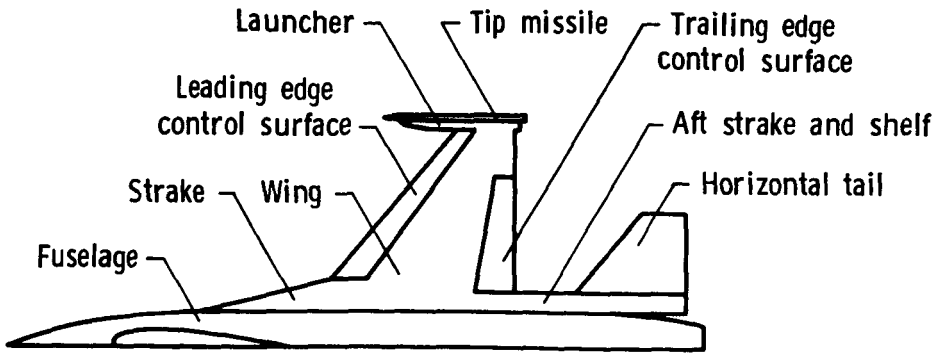

Fig. 4 CAP-TSD modeling of the General Dynamics one-ninth scale F-16C aircraft model.

The bodies include: (1) the tip missile, and (2) the fuselage. Other salient features of the F-16C modeling include 3° linear twist washout for the wing, a leading edge control surface hinge line that is straight but not of constant-percent chord, and 10° anhedral for the horizontal tail. The rather detailed geometry description for the one-ninth scale F-16C aircraft model was obtained from Ref. 20 and the experimental steady pressure data is tabulated in Ref. 21. Parallel calculations were also performed for the wing alone, to investigate the effects of aerodynamic interference by making comparisons with the complete airplane results. These wing-alone calculations were performed for the outer wing panel only, with a plane of symmetry assumed at the wing root.

F-5 Wing/Control Surface Results

Results were obtained for the F-5 wing/control surface configuration to assess the accuracy and efficiency of the CAP-TSD code for oscillatory control surface applications. In these calculations, two Mach number cases were selected. The first case, Case 1 of Table 1, was chosen to have the same freestream conditions as investigated in Refs. 3, 4, and 7. In Case 1, the freestream Mach number was 0.9 and both the mean angle of attack and mean control surface deflection angle were zero. The second case, Case 2 of Table 1, was chosen to assess the performance of CAP-TSD for oscillatory control surface motion with supersonic freestream conditions. In Case 2, the freestream Mach number was 1.1 and again the mean angle of attack and mean control surface deflection angle were both zero. In Cases 1 and 2, both steady and unsteady results were obtained for comparison with the experimental data of Refs. 13 and 15. Steady pressure distributions for these cases were presented and compared with the experimental data in Ref. 7, and therefore are not repeated here. Unsteady pressure results for these cases are described in the following paragraphs.

Case 1. - For Case 1, unsteady results were obtained for the control surface oscillating with amplitude $\delta_1 = 0.471°$ at a reduced frequency of $k = 0.139$. The calculations were performed using only 300 steps per cycle of motion which corresponds to a step size of $\Delta t = 0.07354$. Three cycles of motion were computed to obtain a periodic solution. Unsteady pressure distributions along three span stations of the wing are plotted in Fig. 5 along with the experimental data. The unsteady pressure coefficients along the upper surface are shown in Fig. 5(a); the unsteady pressure coefficients along the lower surface are shown in Fig. 5(b). These coefficients are plotted as real and imaginary components corresponding to the in-phase and out-of-phase unsteady pressure distributions normalized by the amplitude of motion. As shown in Fig. 5(a), there is a calculated shock pulse of moderate strength on the upper surface of the wing near 62% chord at $\bar{n} = 0.18$, 58% chord at $\bar{n} = 0.51$, and 43% chord at $\bar{n} = 0.88$. The shock pulse is due to the motion of the upper surface shock wave and is overpredicted in magnitude in comparison with the experimental data. This is generally what is expected from a conservative inviscid

Table 1 Cases for CAP-TSD analysis.

Configuration	Case	M
F-5 wing/control surface	1	0.9
	2	1.1
F-5 wing/tiptank	3	0.45
F-5 wing/tiptank/pylon/store	4	0.45
DFVLR wing/fuselage/tail	5	0.2
Rockwell canard/wing/fuselage	6	0.8
General Dynamics F-16C aircraft model	7	0.85
	8	0.9
	9	1.1

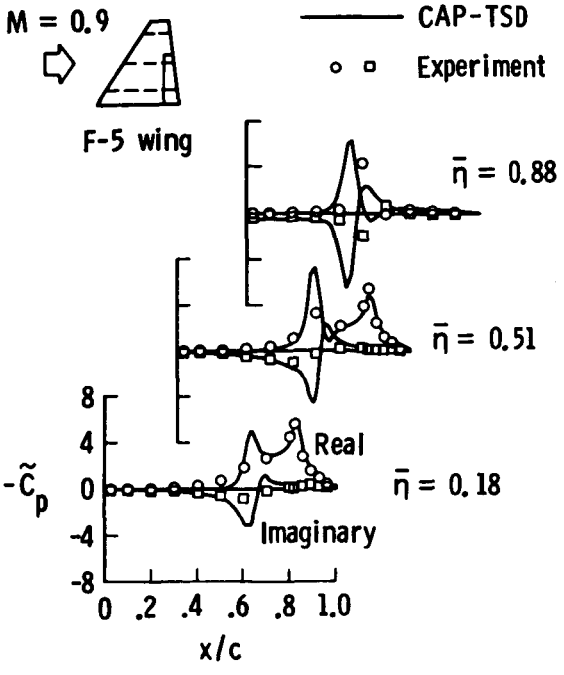

(a) upper surface.

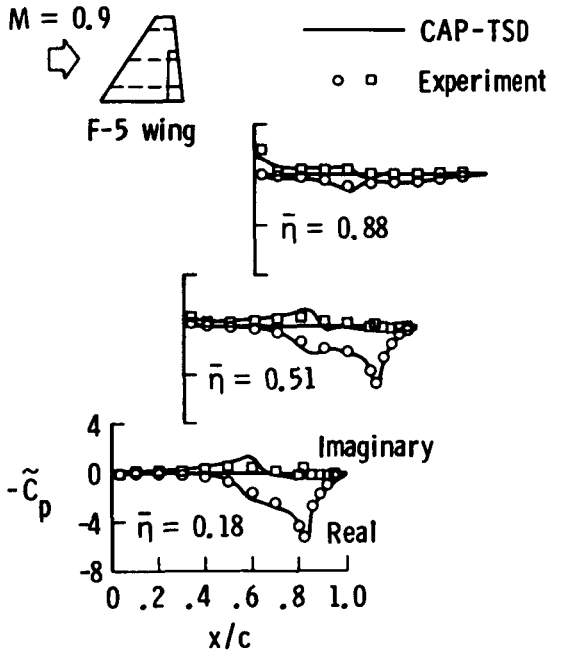

(b) lower surface.

Fig. 5 Comparison between CAP-TSD and experimental unsteady pressure distributions on the F-5 wing due to control surface oscillation at M = 0.9, α_0 = 0°, δ_1 = 0.471°, and k = 0.139.

potential flow code. For cases such as this, the inclusion of the nonisentropic effects[22] and viscous effects[23] could be expected to improve the correlation between calculation and experiment. Overall, the CAP-TSD results generally agree well with the experimental data, especially in predicting the control surface pressures and the hinge-line singularity at 82% chord (Figs. 5(a) and 5(b)).

Case 2. - For Case 2, unsteady results were obtained for the control surface oscillating with amplitude δ_1 = 0.45° at a reduced frequency of k = 0.118. Similar to Case 1, the calculations were also performed using 300 steps per cycle of motion which corresponds to a step size of Δt = 0.08875. Only two cycles of motion were required to obtain a periodic solution. Calculations for the third cycle of motion produced results that were identical to the second cycle results, to plotting accuracy. This faster convergence is due to the lack of upstream signal propagation resulting from the supersonic nature of the flow. Figure 6 shows a comparison of CAP-TSD unsteady pressures with the experimental data. Upper surface pressure distributions are shown in Fig. 6(a); lower surface pressure distributions are shown in Fig. 6(b). The CAP-TSD results indicate that the pressures on the control surface are nearly in-phase with the motion since the imaginary components are very small in comparison to the real components. Also, the pressures are zero outside of the domain of influence of the control surface which is expected for supersonic flow. The CAP-TSD results are in very good agreement with the experimental pressure data along both the upper (Fig. 6(a)) and lower (Fig. 6(b)) surfaces of the wing.

F-5 Wing/Tiptank/Pylon/Store Results

Results were obtained for the F-5 wing/tiptank/pylon/store configuration to assess the CAP-TSD modeling for multiple body geometries. In these calculations, two cases were selected to investigate the effects of component aerodynamic interference. The first case, Case 3 of Table 1, considers results for the F-5 wing with and without the tiptank included in the calculation. Comparisons between these two sets of results reveal the interference effects of the tiptank on wing pressures. The second case, Case 4 of Table 1, considers results for the F-5 wing/tiptank geometry both with and without the pylon and store included in the calculation. Comparisons between these results reveal further interference effects on wing pressures. In both Cases 3 and 4, the freestream Mach number was selected as M = 0.45 for direct comparison with the published subsonic experimental pressure data of Refs. 16 and 17. In these calculations, both steady and unsteady results were obtained for the wing at zero mean angle of attack. The unsteady calculations were performed for the configuration pitching harmonically at a reduced frequency of k = 0.147. The configuration was forced to pitch about a line perpendicular to the root at 15% chord from the wing apex. The results were obtained using 300 steps per cycle of motion which corresponds to a step size of Δt = 0.07135.

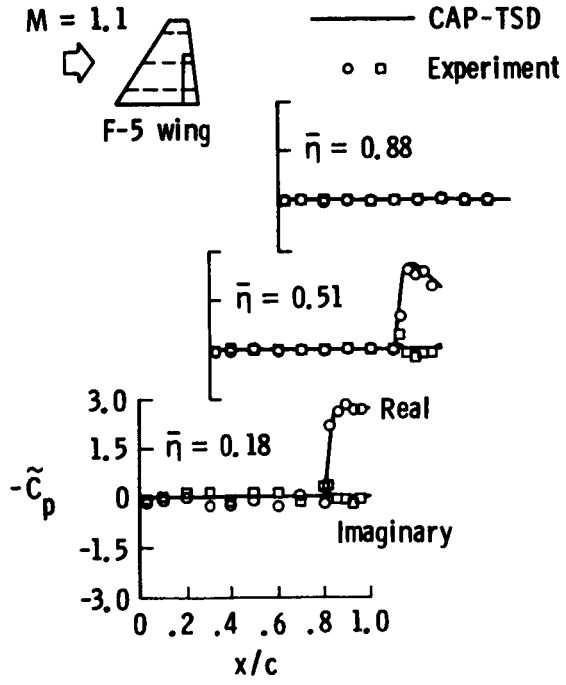

(a) upper surface.

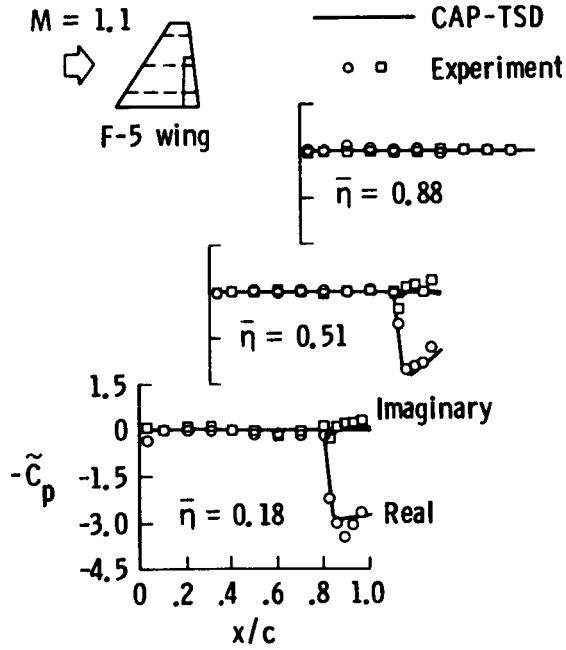

(b) lower surface.

Fig. 6 Comparison between CAP-TSD and experimental unsteady pressure distributions on the F-5 wing due to control surface oscillation at M = 1.1, α_0 = 0°, δ_1 = 0.45°, and k = 0.118.

Case 3. - For Case 3, steady pressure distributions on the tiptank are presented first, to assess the accuracy of the CAP-TSD body modeling. As shown in Fig. 7, two sets of pressures are plotted corresponding to inboard (θ = 157.5°) and outboard (θ = 22.5°) longitudinal lines along the tiptank. These pressure distributions show expansions near the fore and aft maximum diameter locations as well as a compression near the area-ruled middle region. The calculated tiptank pressures are in very good agreement with the experimental data which validates the CAP-TSD body modeling.

Unsteady pressure distributions for Case 3 are presented in Fig. 8 for two span stations of the F-5 wing. Figure 8(a) shows chordwise pressures along 98% semispan and Fig. 8(b) shows chordwise pressures along 51% semispan. These pressures are plotted as real and imaginary components of the unsteady lifting pressure, normalized by the amplitude of motion. Two sets of calculated results are presented corresponding to the wing with and without the tiptank included in the calculation. As shown in Fig. 8(a), inclusion of the tiptank increased the magnitude of the real part which brings the calculated results into good general agreement with the wing/tiptank experimental data in the midchord region. The interference effect of the tiptank on the wing unsteady pressures is largest near the wing tip (Fig. 8(a)), as expected, and attenuates inboard along the span as shown in Fig. 8(b). Here the increase in the real part of the unsteady lifting pressure is much less than that predicted near the tip.

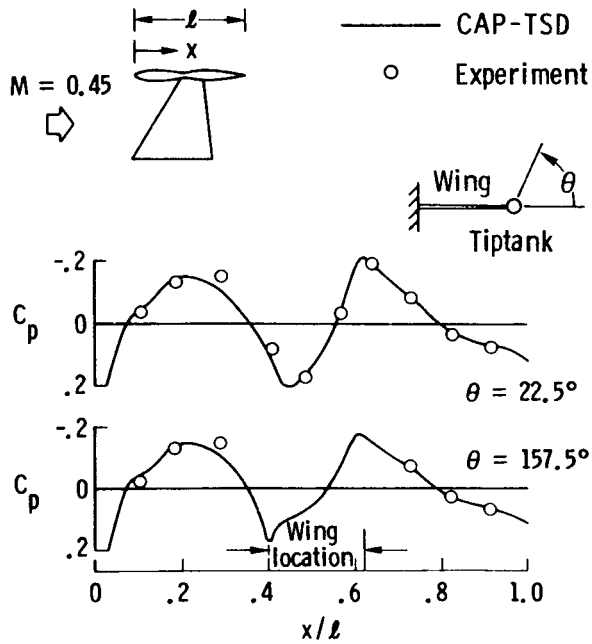

Fig. 7 Comparison between CAP-TSD and experimental steady pressure distributions on the tiptank of the F-5 wing/tiptank configuration at M = 0.45 and α_0 = 0°.

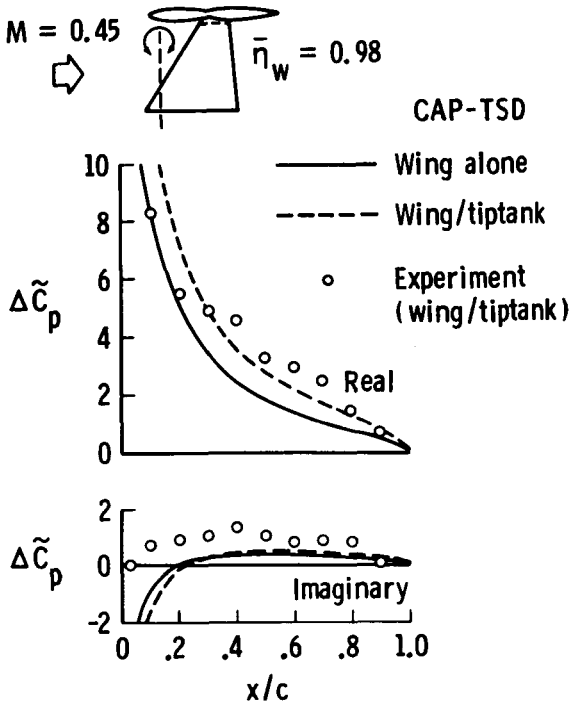

(a) $\bar{\eta}_w$ = 0.98.

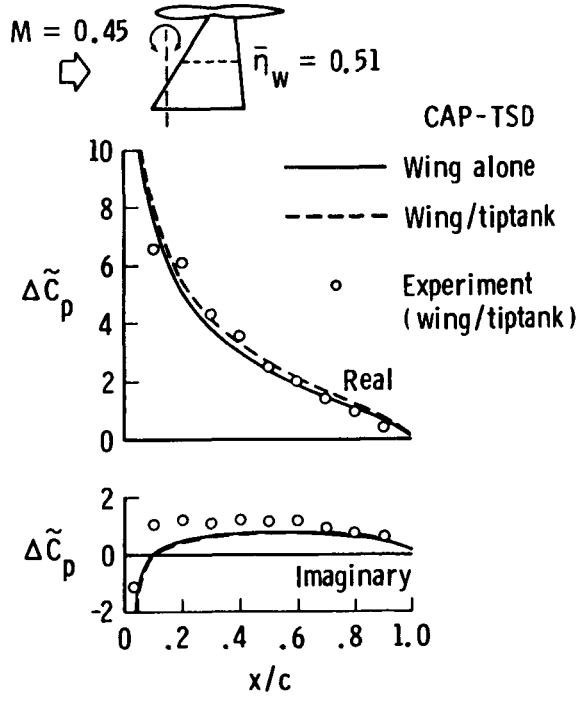

(b) $\bar{\eta}_w$ = 0.51.

Fig. 8 Comparison between CAP-TSD and experimental unsteady pressure distributions on the wing of the F-5 wing/tiptank configuration at M = 0.45, α_0 = 0°, and k = 0.147.

Case 4. - For Case 4, steady pressure distributions on the wing are presented in Fig. 9. Figure 9(a) shows chordwise pressures along 72% semispan, which is slightly inboard of the pylon location, and Fig. 9(b) shows chordwise pressures along 18% semispan. Two sets of calculated and experimental results are plotted corresponding to the wing/tiptank configuration with and without the pylon/store included. As shown in the lower part of Fig. 9(a), inclusion of the pylon and store significantly increased (negatively) the lower surface pressures from the wing leading edge to approximately 60% chord. The effect on the upper surface pressures is negligible, as shown in the upper part of Fig. 9(a). The calculated steady pressures for cases with and without the pylon/store compare very well with the experimental data. The interference effect of the pylon and store on the wing lower surface steady pressures is largest in the pylon location region, as expected. The effect attenuates along the span and is small at the 18% semispan location (Fig. 9(b)).

Unsteady pressure distributions for Case 4 are presented in Fig. 10 for the same two span stations of the F-5 wing. Two sets of calculated and experimental results are again plotted corresponding to the wing/tiptank configuration with and without the pylon/store. As shown in the upper part of Fig. 10(a), inclusion of the pylon and store increased the real component of the unsteady lifting pressure, similar to the interference effect of the tiptank on the wing unsteady pressures (Fig. 8(a)). The CAP-TSD results are in good agreement with the experimental pressure data in predicting the aerodynamic interference effect of the pylon/store. Similar to the steady-state example of Fig. 9, the effect attenuates in the spanwise direction and is very small inboard at the 18% semispan location as shown in Fig. 10(b).

DFVLR Wing/Fuselage/Tail Results

Results were obtained for the DFVLR wing/fuselage/tail configuration to assess the accuracy and utility of CAP-TSD for multiple lifting surface and fuselage applications. In these calculations, one case was considered which is Case 5 of Table 1. In Case 5, the freestream Mach number was selected as M = 0.2 for comparison with the low-speed experimental steady pressure data of Ref. 18. The angle of attack of the wing was 0.25°. The angle of attack for the tail and fuselage was 0.15°. For this case as well as for all of the remaining complex configurations, only steady-state comparisons with experiment are given.

Case 5. - For Case 5, comparisons of CAP-TSD and experimental steady pressure distributions on the upper surfaces of the wing and tail are presented in Fig. 11. Chordwise pressures along three span stations of the wing and along one span station of the tail were selected for comparison with the data. As shown in Fig. 11, the CAP-TSD results compare very well with the experimental data along both lifting surfaces except in the vicinity of the

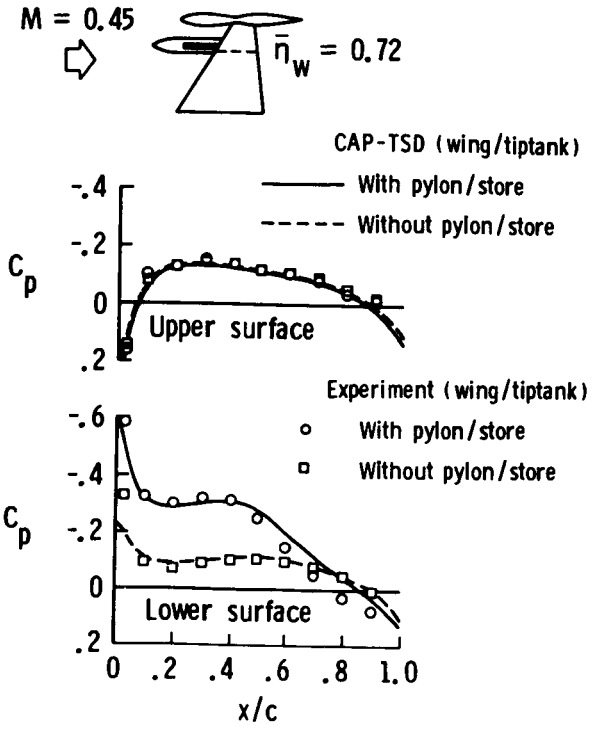

(a) $\bar{\eta}_w$ = 0.72.

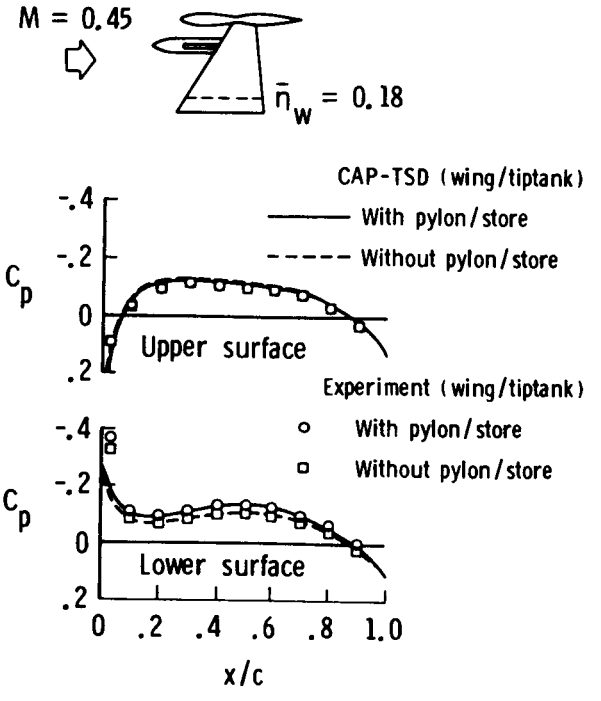

(b) $\bar{\eta}_w$ = 0.18.

Fig. 9 Comparison between CAP-TSD and experimental steady pressure distributions on the wing of the F-5 wing/tiptank configuration both with and without pylon/store at M = 0.45 and α_0 = 0°.

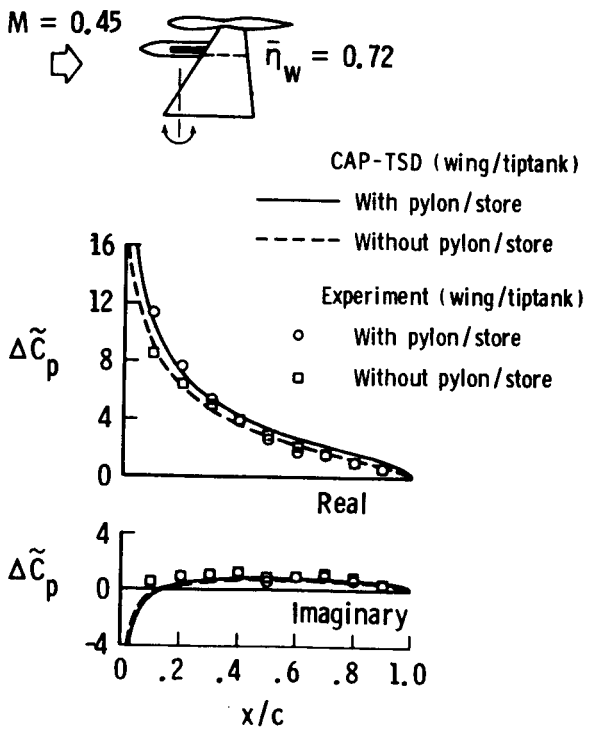

(a) $\bar{\eta}_w$ = 0.72.

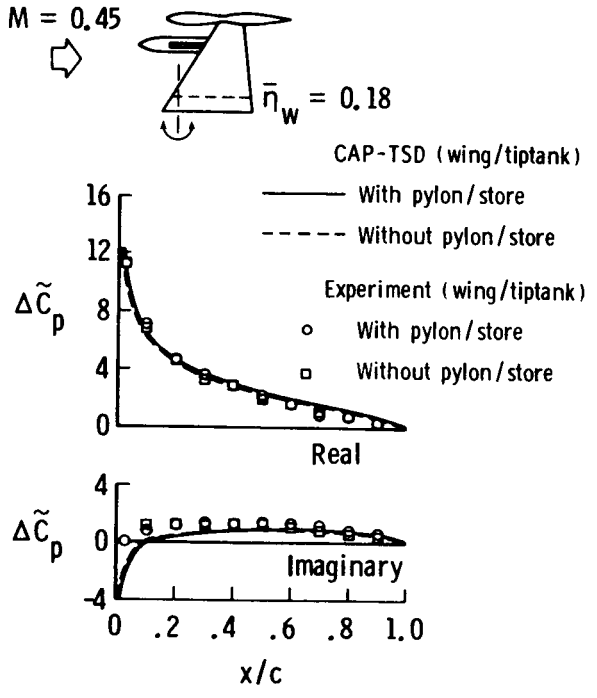

(b) $\bar{\eta}_w$ = 0.18.

Fig. 10 Comparison between CAP-TSD and experimental unsteady pressure distributions on the wing of the F-5 wing/tiptank configuration both with and without pylon/store at M = 0.45, α_0 = 0°, and k = 0.147.

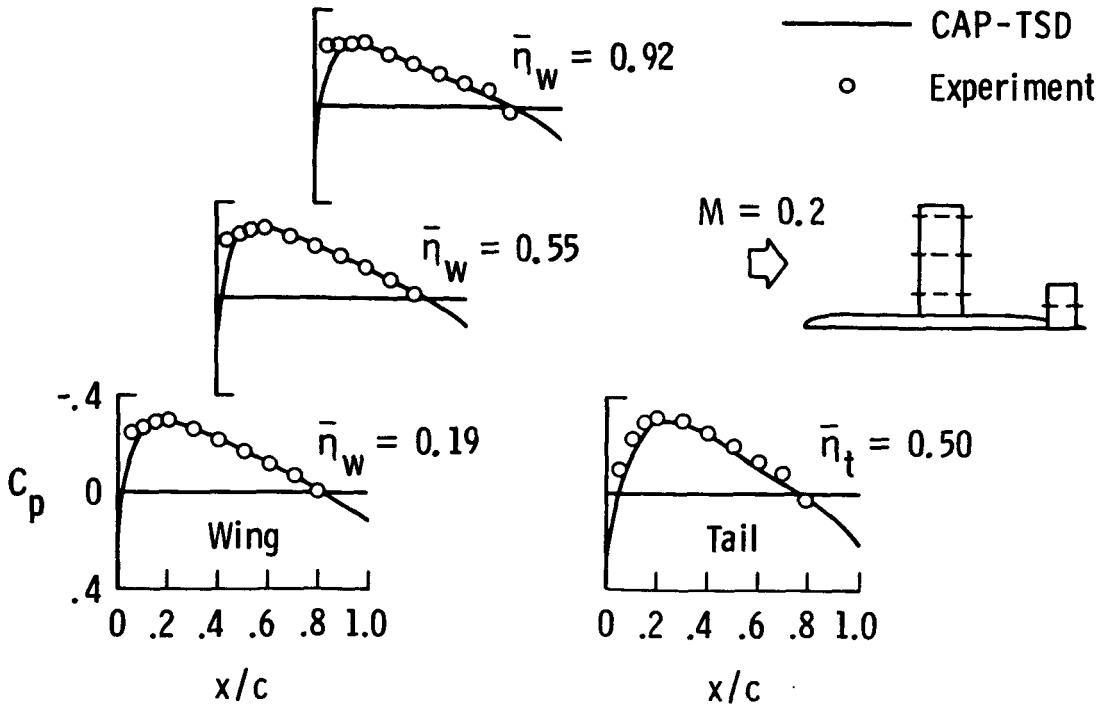

Fig. 11 Comparison between CAP-TSD and experimental steady pressure distributions on the wing and tail of the DFVLR wing/fuselage/tail configuration at M = 0.2, α_w = 0.25°, and $\alpha_f = \alpha_t$ = 0.15°.

wing leading edge. Figure 12 shows a similar comparison between CAP-TSD and experiment for the fuselage of the DFVLR configuration. Two sets of longitudinal pressures are plotted corresponding to the fuselage upper centerline (θ = 90°) and to a line that passes close to the wing-fuselage junction (θ = 20°). The calculated pressure distributions are again in very good agreement with the experimental data

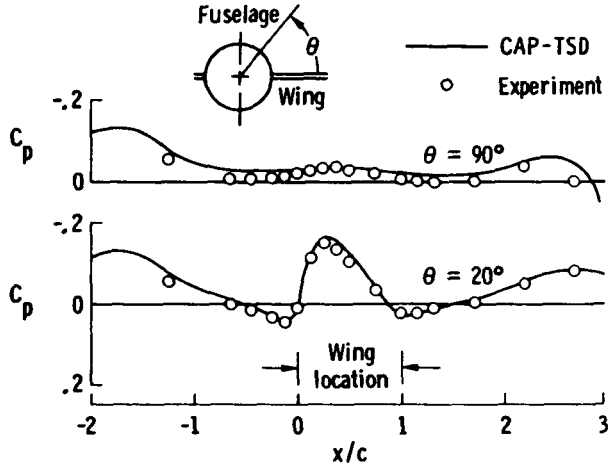

Fig. 12 Comparison between CAP-TSD and experimental steady pressure distributions on the fuselage of the DFVLR wing/fuselage/tail configuration at M = 0.2, α_w = 0.25°, and $\alpha_f = \alpha_t$ = 0.15°.

which validates the CAP-TSD code for application to multiple-component configurations such as the DFVLR wing/fuselage/tail.

Rockwell Canard/Wing/Fuselage Results

Results were obtained for the Rockwell canard/wing/fuselage configuration to further assess CAP-TSD for multiple lifting surface and fuselage applications. In these calculations, one case was considered which is Case 6 of Table 1. In Case 6, the freestream Mach number was M = 0.8 for comparison with the experimental steady pressure data of Ref. 19. The angle of attack for both the canard and wing was 2.05°. For the wing, this angle is added to the incidence and twist so that the root and tip are effectively at 6.05° and 1.05°, respectively.

Case 6. - For Case 6, comparisons of CAP-TSD and experimental steady pressure distributions on the canard and wing are plotted in Fig. 13. Chordwise pressures along one span station of the canard and along three span stations of the wing were selected for comparison with the data. As shown in Fig. 13, the CAP-TSD pressures are in favorable agreement with the experimental data along both lifting surfaces. The small differences between calculation and experiment in the wing upper surface trailing edge region, are due to flow separation. The overpredicted pressures along the lower surface of both the canard and the wing, aft of approximately 85% chord, are due to viscous effects. Of course, flow separation and viscous effects are outside the scope of the present capability.

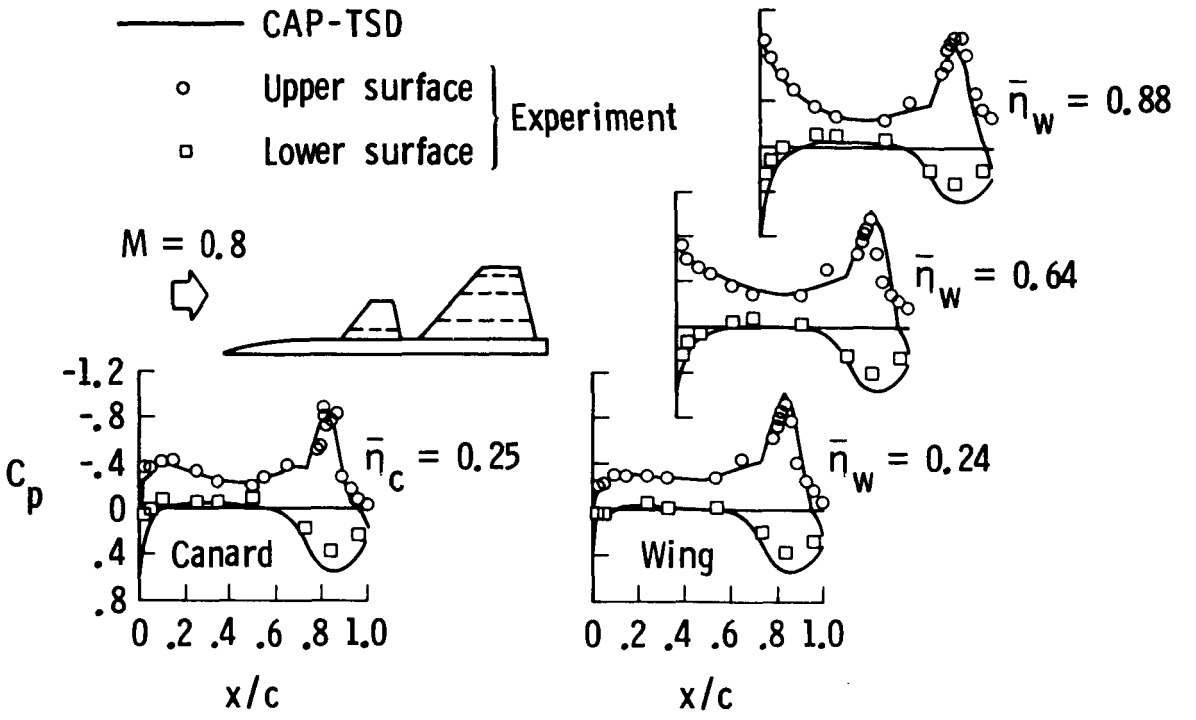

Fig. 13 Comparison between CAP-TSD and experimental steady pressure distributions on the canard and wing of the Rockwell canard/wing/fuselage configuration at M = 0.8, $\alpha_c = \alpha_w = 2°$, and $\alpha_f = 0°$.

General Dynamics F-16C Aircraft Model Results

Results were obtained for the General Dynamics one-ninth scale F-16C aircraft model to demonstrate application of CAP-TSD to a realistic configuration. In these calculations, three cases were considered corresponding to three values of freestream Mach number. The three cases are referred to as Cases 7, 8, and 9 of Table 1, which correspond to M = 0.85, 0.9, and 1.1, respectively. In each case, CAP-TSD results were obtained for the F-16C aircraft at approximately 2.3° angle of attack and with the leading edge control surface of the wing deflected upwards 2° for comparison with the experimental steady pressure data of Ref. 21. These steady pressure comparisons are made to assess the accuracy of CAP-TSD for complete airplane applications. There are no unsteady experimental data to validate the CAP-TSD code for time-accurate F-16C calculations. Nonetheless, an unsteady calculation was performed for Case 8, to demonstrate the time-accurate capability. For simplicity, the calculation was performed for a rigid pitching motion where the entire F-16C aircraft was forced to oscillate about the model moment reference axis at a reduced frequency of k = 0.1. The oscillation amplitude was chosen as α_1 = 0.5°, and 300 steps per cycle of motion were computed corresponding to Δt = 0.1047. Parallel results were also obtained for the wing alone to investigate the aerodynamic interference effects of the additional aircraft components on wing unsteady pressures.

For the F-16C configuration, all of the calculations for Cases 7-9 were performed on a grid which contained 324,000 points. Since the grid is Cartesian, it was relatively easy to generate, even for such a complex configuration as the F-16C aircraft. Also, the calculations required only about 0.88 CPU seconds per time step and thirteen million words of memory on the CDC VPS-32 computer.

Case 7. - For Case 7, steady pressure comparisons for the F-16C aircraft model are presented in Fig. 14 for three span stations of the wing and one span station of the tail. These calculations were performed to assess the CAP-TSD complete aircraft modeling first for subsonic flow conditions. For this case (M = 0.85), the flow is mostly subcritical and the CAP-TSD results are in good agreement with the experimental data. The wing pressure distributions indicate the effects of the leading edge control surface hinge line and that the wing carries lift. The tail, although at angle of attack, carries relatively little lift in comparison with the wing. This is because the wing induces a downwash on the tail which reduces its effective angle of attack and consequently reduces the tail lift.

Case 8. - For Case 8, steady pressure comparisons are presented in Fig. 15 for the same span stations as shown for Case 7. These calculations were performed to assess the

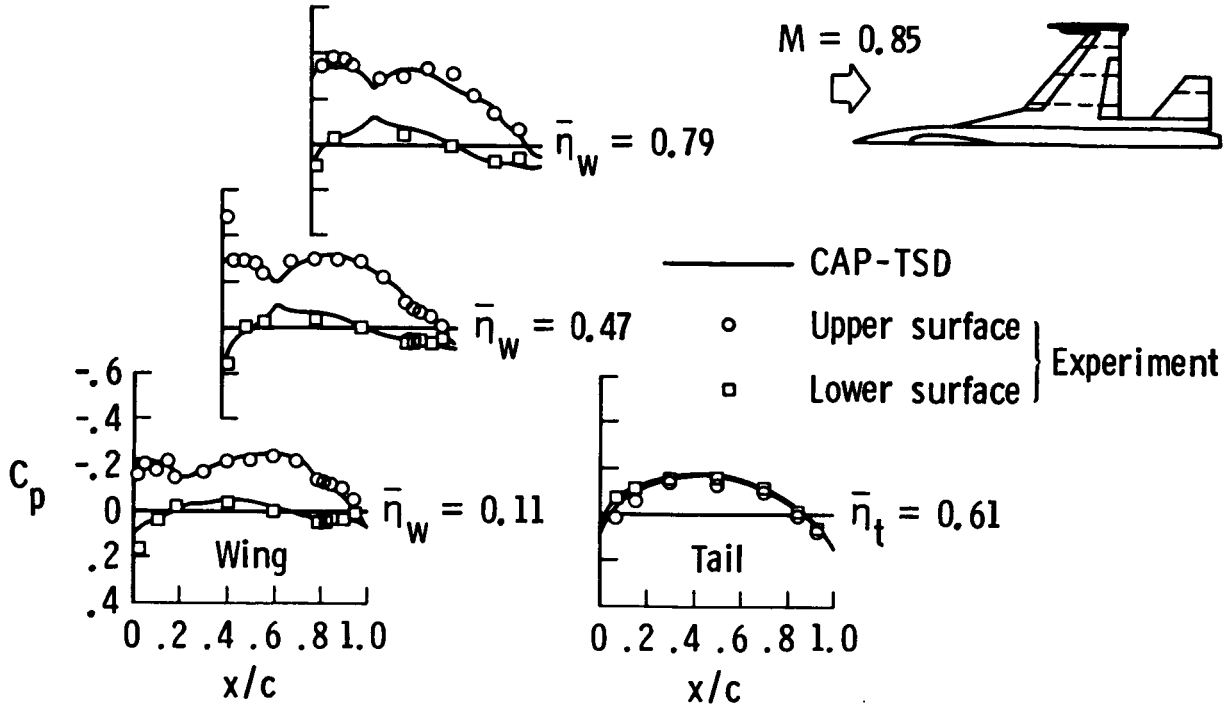

Fig. 14 Comparison between CAP-TSD and experimental steady pressure distributions on the wing and tail of the F-16C aircraft model at M = 0.85 and α_0 = 2.32°.

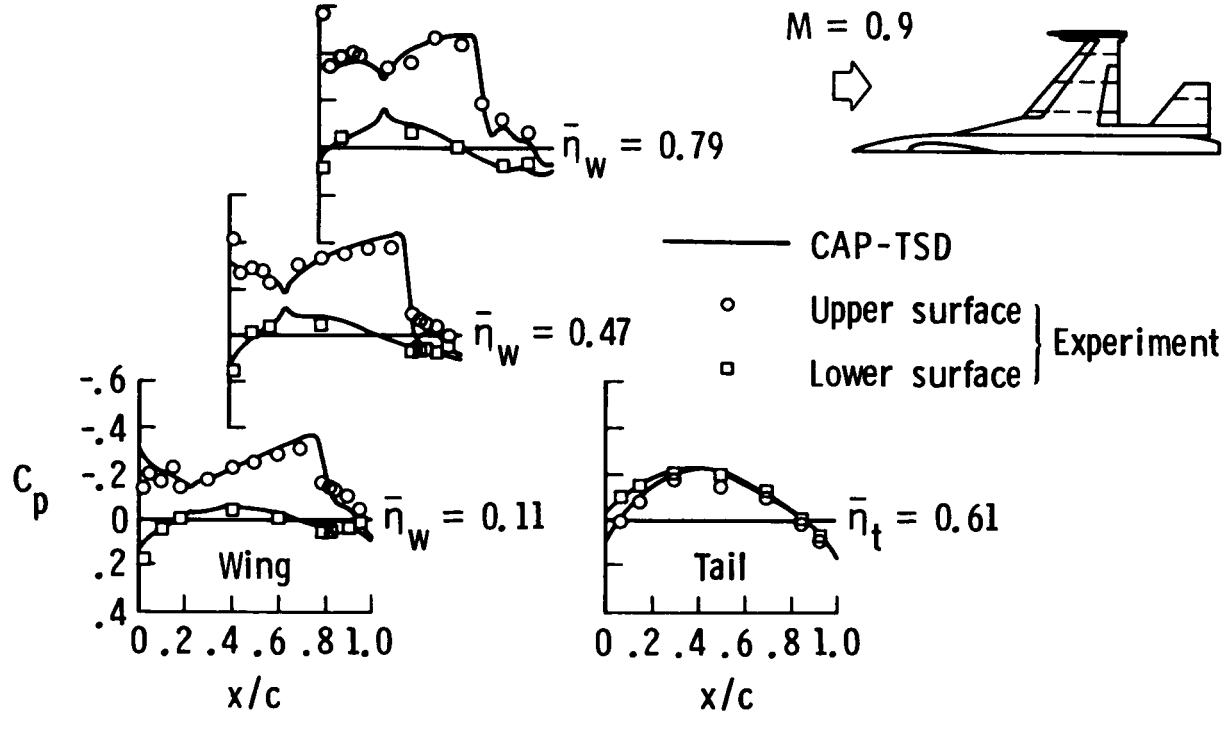

Fig. 15 Comparison between CAP-TSD and experimental steady pressure distributions on the wing and tail of the F-16C aircraft model at M = 0.9 and α_0 = 2.38°.

CAP-TSD complete aircraft modeling for transonic conditions. In this case (M = 0.9), there is a moderately strong shock wave on the upper surface of the wing and the CAP-TSD pressures again generally agree well with the experimental pressures. The shock is slightly overpredicted in strength and located slightly aft of the experimental location which is expected from a conservative inviscid potential flow code. Similar to Case 1, the inclusion of the nonisentropic effects[22] and viscous effects[23] could be expected to improve the correlation between calculation and experiment. For the tail, the flow is predominantly subcritical and the CAP-TSD pressures agree well with the experimental data.

Unsteady pressure distributions for Case 8 are shown in Fig. 16 for the entire F-16C aircraft undergoing a rigid pitching motion. The wing and tail upper surface results are shown in Fig. 16(a) and the lower surface results are shown in Fig. 16(b). These unsteady pressure results are presented at the same span stations as the steady-state results (Fig. 15). Two sets of calculated pressures are compared corresponding to complete airplane and wing alone modeling. As shown in Fig. 16(a), there is a relatively large shock pulse in the real part of the wing upper surface pressures. This shock pulse is of larger magnitude and is located further downstream in the complete airplane model. These features are attributed to a stronger steady-state shock on the upper surface of the wing produced by the accelerated flow about the fuselage and the launcher/tip missile. The unsteady pressures near the leading edge of the wing are also generally of larger magnitude for the complete airplane. For the tail, the unsteady pressures are relatively small in comparison with the wing pressures and thus were plotted on an expanded scale. The tail is located considerably aft of the pitch axis and thus its motion is plunge dominated which results in smaller airloads for the low value of k considered. Furthermore, these pressures are nearly 90° out of phase with the aircraft motion since the real components are small compared to the imaginary components. As shown in Fig. 16(b), the complete airplane and wing alone results on the wing lower surface show much smaller differences than the results for the wing upper surface due to the subcritical nature of the flow.

Case 9. - For Case 9, steady pressure results are presented in Fig. 17 for the F-16C aircraft model at M = 1.1. These calculations were performed to assess the CAP-TSD complete aircraft modeling for supersonic freestream conditions. For this case, the flow is mostly supersonic and the CAP-TSD results are in favorable agreement with the experimental data for both the wing and tail. The steady pressure levels are generally well predicted except outboard along the wing leading edge control surface. This discrepancy may be due to a vortex that is produced outboard along the leading edge. Of course, vortex flows are outside the scope of the present capability.

Concluding Remarks

A transonic unsteady aerodynamic and aeroelasticity code called CAP-TSD has been developed for application to realistic aircraft configurations. The name CAP-TSD is an acronym for Computational Aeroelasticity Program - Transonic Small Disturbance. The new code now permits the calculation of unsteady flows about complete aircraft configurations for aeroelastic analysis in the flutter critical transonic speed range. The CAP-TSD code uses a time-accurate approximate factorization (AF) algorithm for solution of the unsteady transonic small-disturbance equation. The AF algorithm has been shown to be very efficient for steady or unsteady transonic flow problems. It can provide accurate solutions in only several hundred time steps yielding a significant computational cost savings when compared to alternative methods. For reasons of practicality and affordability, an efficient algorithm and a fast computer code are requirements for realistic aircraft applications.

Results were presented for several complex aircraft configurations which demonstrated the geometrical applicability of CAP-TSD. The code can treat configurations with arbitrary combinations of lifting surfaces and bodies including canard, wing, tail, control surfaces, tip launchers, pylons, fuselage, stores, and nacelles. Most of the cases presented are steady-state calculations for comparison with available experimental data.

Calculations presented for the F-5 wing with an inboard trailing edge oscillating control surface demonstrated the accuracy and efficiency of CAP-TSD for unsteady flows with subsonic and supersonic freestream conditions. These results compared well with the experimental data. Steady pressure distributions obtained for the DFVLR wing/fuselage/tail and the Rockwell canard/wing fuselage were also in good agreement with the experimental pressure data. The favorable comparisons thus verified the CAP-TSD coding for multiple lifting surface and fuselage geometries and also demonstrated the accuracy of the program for such applications. Steady and unsteady calculations for the F-5 wing with a tiptank and underwing pylon/store further demonstrated CAP-TSD geometry capabilities. Comparisons of pressure distributions for combinations of F-5 components revealed aerodynamic interference effects on wing pressures. These calculated results were in good agreement with the experimental pressure data which further assessed CAP-TSD for multiple component applications with mutual interference effects.

Finally, results were presented for the General Dynamics one-ninth scale F-16C aircraft model which demonstrated application to a realistic configuration. The F-16C components that were modeled with CAP-TSD include the wing with leading and trailing edge control surfaces; a highly-swept strake, aft strake, and shelf surface; the tip launcher and missile; the horizontal tail; and the fuselage. Steady

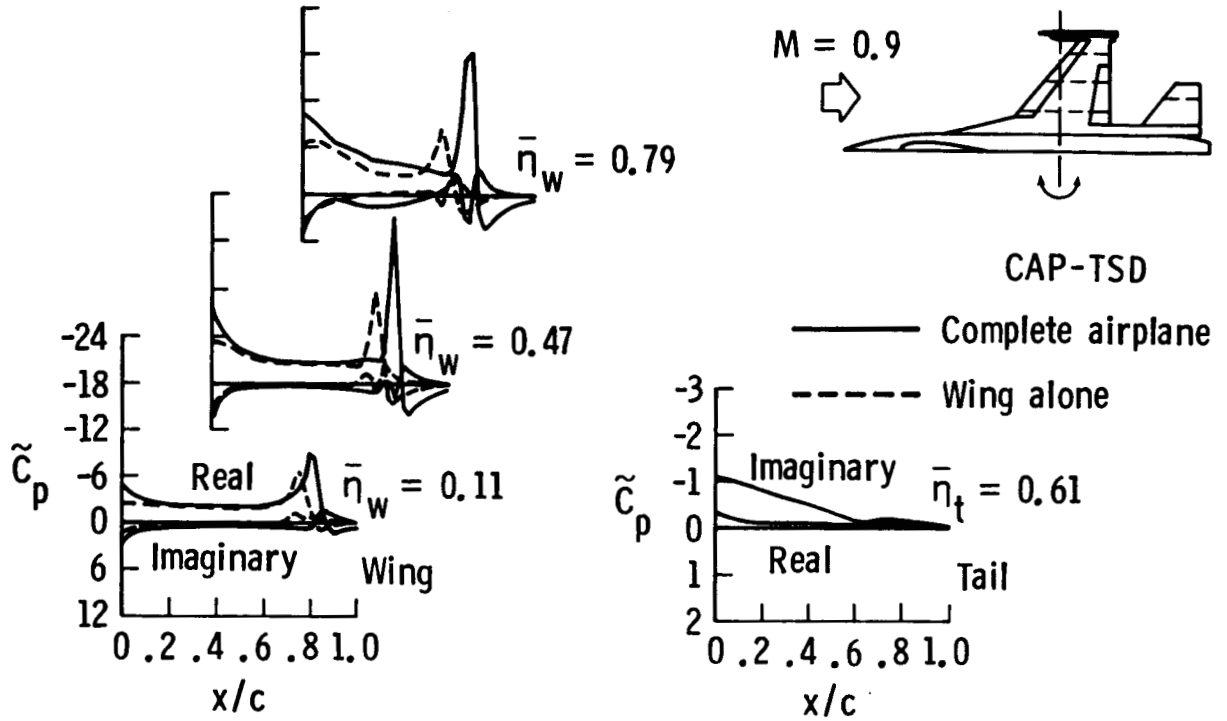

(a) upper surfaces.

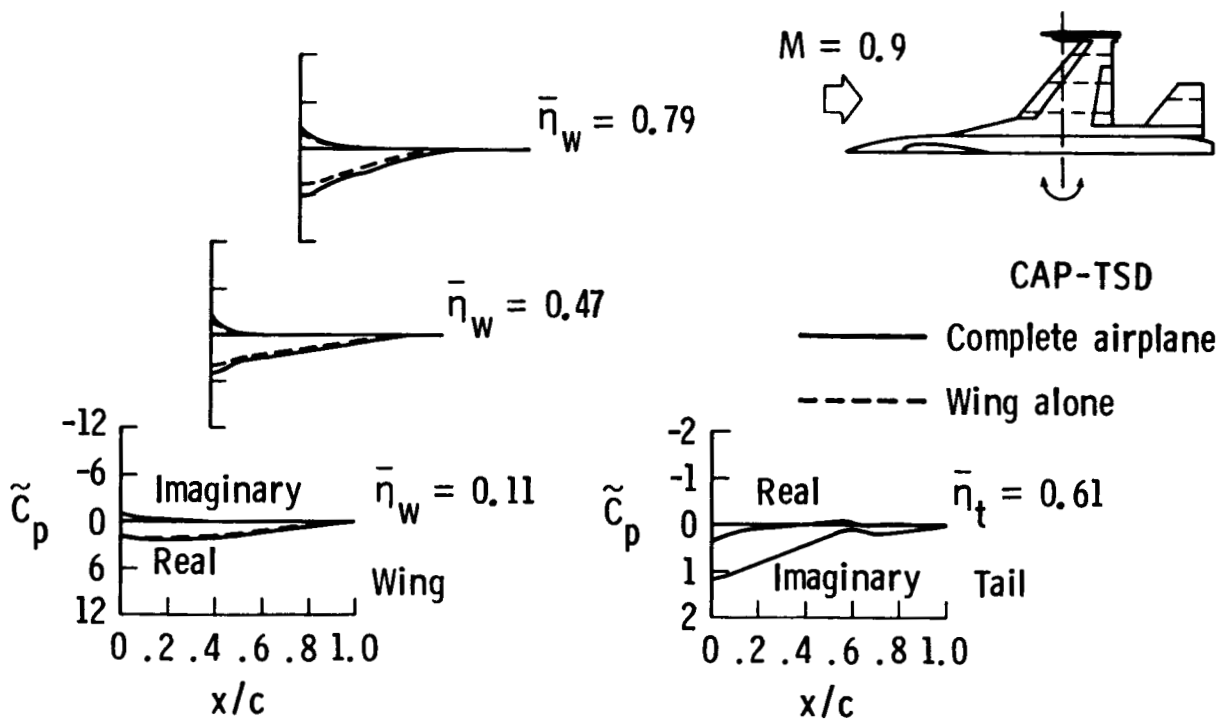

(b) lower surfaces.

Fig. 16 CAP-TSD unsteady pressure distributions on the wing and tail of the F-16C aircraft model due to complete airplane rigid pitching at M = 0.9, α_0 = 2.38°, α_1 = 0.5°, and k = 0.1.

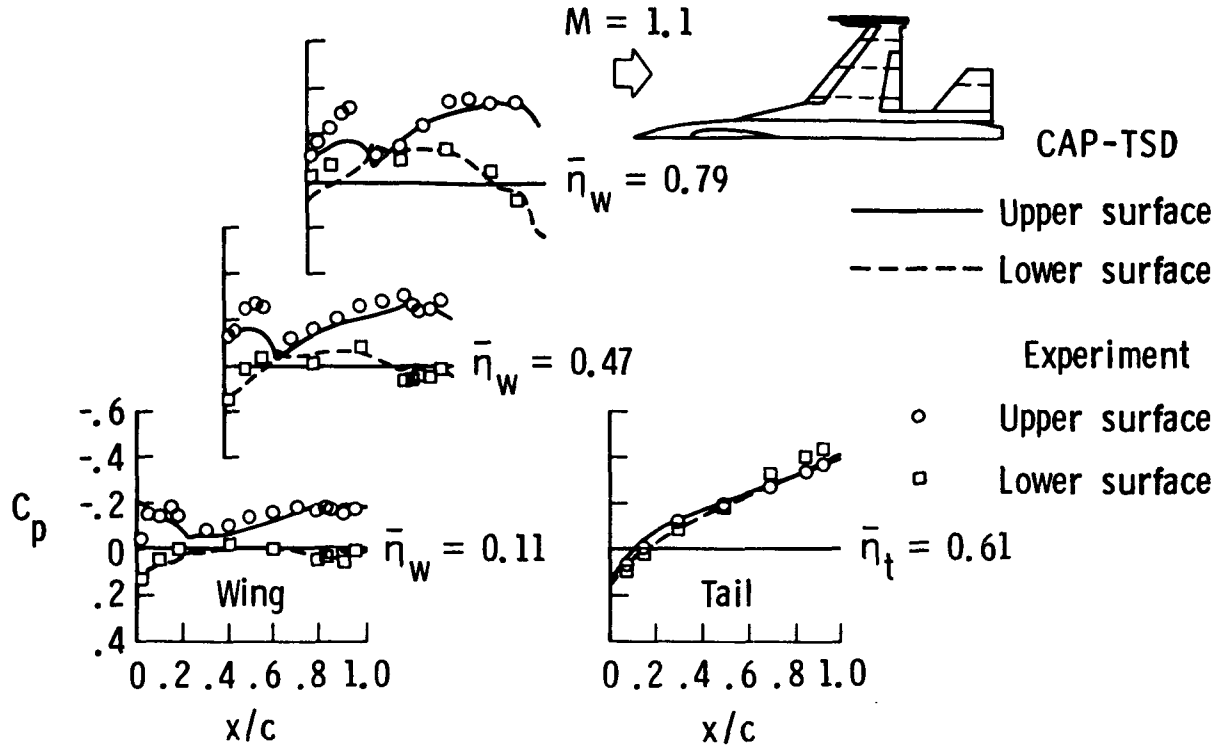

Fig. 17 Comparison between CAP-TSD and experimental steady pressure distributions on the wing and tail of the F-16C aircraft model at M = 1.1 and α_0 = 2.31°.

results at both subsonic and supersonic freestream conditions compared well with the experimental data. Unsteady results for the entire F-16C aircraft undergoing a rigid pitching motion were presented. Comparisons with parallel wing alone results revealed aerodynamic interference effects of the additional aircraft components on wing unsteady pressures. These effects emphasize the importance of including all components in the calculation. The CAP-TSD code thus provides the capability of modeling complete aircraft configurations for realistic transonic and supersonic unsteady aerodynamic and aeroelastic analyses.

References

[1]Edwards, J. W.; and Thomas, J. L.: "Computational Methods for Unsteady Transonic Flows," AIAA Paper No. 87-0107, Presented at the AIAA 25th Aerospace Sciences Meeting, Reno, Nevada, January 12-15, 1987.

[2]Borland, C. J.; and Rizzetta, D. P.: "Nonlinear Transonic Flutter Analysis," AIAA Journal, Vol. 20, November 1982, pp. 1606-1615.

[3]Guruswamy, Guru P.; and Goorjian, Peter M.: "Efficient Algorithm for Unsteady Transonic Aerodynamics of Low-Aspect-Ratio Wings," Journal of Aircraft, Vol. 20, March 1985, pp. 193-199.

[4]Borland, C. J.; and Sotomayer, W. A.: "An Algorithm for Unsteady Transonic Flow About Tapered Wings," AIAA Paper No. 84-1567, Presented at the AIAA 17th Fluid Dynamics, Plasmadynamics, and Lasers Conference, Snowmass, Colorado, June 25-27, 1984.

[5]Bennett, Robert M.; Wynne, Eleanor C.; and Mabey, Dennis G.: "Calculation of Transonic Steady and Oscillatory Pressures on a Low Aspect Ratio Model and Comparison with Experiment," Paper 85-17, Presented at the Second International Symposium on Aeroelasticity and Structural Dynamics, Technical University of Aachen, Germany, April 1-3, 1985.

[6]Guruswamy, Guru P.; Goorjian, Peter M.; Ide, Hiroshi; and Miller, Gerry D.: "Transonic Aeroelastic Analysis of the B-1 Wing," Journal of Aircraft, Vol. 23, July 1986, pp. 547-553.

[7]Batina, J. T.: "An Efficient Algorithm for Solution of the Unsteady Transonic Small-Disturbance Equation," AIAA Paper No. 87-0109, Presented at the AIAA 25th Aerospace Sciences Meeting, Reno, Nevada, January 12-15, 1987. (Also available as NASA TM 89014, December 1986).

[8]Batina, J. T.: "Unsteady Transonic Flow Calculations for Interfering Lifting Surface Configurations," Journal of Aircraft, Vol. 23, May 1986, pp. 422-430.

[9]Batina, J. T.: "Unsteady Transonic Flow Calculations for Wing-Fuselage Configurations," Journal of Aircraft, Vol. 23, December 1986, pp. 897-903.

[10]Boppe, C. W.; and Stern, M. A.: "Simulated Transonic Flows for Aircraft with Nacelles, Pylons, and Winglets," AIAA Paper No. 80-0130, Presented at the AIAA 18th Aerospace Sciences Meeting, Pasadena, CA, January 14-16, 1980.

[11]Shankar, Vijaya; and Malmuth, Norman: "Computational and Simplified Analytical Treatment of Transonic Wing/Fuselage/Pylon/Store Interactions," Journal of Aircraft, Vol. 18, August 1981, pp. 631-637.

[12]Whitlow, W., Jr.: "Characteristic Boundary Conditions for Three Dimensional Transonic Unsteady Aerodynamics," NASA TM 86292, October 1984.

[13]Tijdeman, H.; Van Nunen, J. W. G.; Kraan, A. N.; Persoon, A. J.; Poestkoke, R.; Roos, R.; Schippers, P.; and Siebert, C. M.: "Transonic Wind Tunnel Tests on an Oscillating Wing with External Stores," AFFDL-TR-78-194, December 1978.

[14]Bennett, R. M.; Bland, S. R.; Batina, J. T.; Gibbons, M. D.; and Mabey, D. G.: "Calculation of Steady and Unsteady Pressures on Wings at Supersonic Speeds with a Transonic Small-Disturbance Code," AIAA Paper No. 87-0851, Presented at the AIAA/ASME/ASCE/AHS 28th Structures, Structural Dynamics, and Materials Conference, Monterey, CA, April 6-8, 1987.

[15]Persoon, A. J.; Roos, R.; and Schippers, P.: "Transonic and Low Supersonic Wind-Tunnel Tests on a Wing with Inboard Control Surface," AFWAL-TR-80-3146, December 1980.

[16]Renirie, L.: "Analysis of Measured Aerodynamic Loads on an Oscillating Wing-Store Combination in Subsonic Flow," NLR MP 74026 U, September 1974.

[17]Bennekers, B.; Roos, R.; and Zwann, R. J.: "Calculation of Aerodynamic Loads on Oscillating Wing/Store Combinations in Subsonic Flow," NLR MP 74028 U, September 1974.

[18]Korner, H.; and Schroder, W.: "Druckverteilungs- und Kraftmessungen an einer Flugel-Rumpf-Leitwerk-Anordnung," DFVLR-IB-080-72/13, 1972.

[19]Stewart, V. R.: "Evaluation of a Propulsive Wing/Canard Concept at Subsonic and Supersonic Speeds," Rockwell International Report NR82H-85, February 1983.

[20]Fox, M. C.; and Feldman, C. S.: "Model and Test Information Report, 1/9-Scale F-16C and F-16D Force and Loads Model," General Dynamics Report 16PR2179, January 1982.

[21]Feldman, C. S.: "Wind Tunnel Data Report, 1/9-Scale F-16C Pressure Loads Test," General Dynamics Report 16PR2252, July 1982.

[22]Gibbons, M. D.; Whitlow, W., Jr.; and Williams, M. H.: "Nonisentropic Unsteady Three Dimensional Small Disturbance Potential Theory," AIAA Paper No. 86-0863, Presented at the AIAA/ASME/ASCE/AHS 27th Structures, Structural Dynamics, and Materials Conference, San Antonio, Texas, May 19-21, 1986.

[23]Howlett, J. T.: "Efficient Self-Consistent Viscous-Inviscid Solutions for Unsteady Transonic Flow," AIAA Paper No. 85-0482, Presented at the AIAA 23rd Aerospace Sciences Meeting, Reno, NV, January 14-17, 1985.

Standard Bibliographic Page

1. Report No.	2. Government Accession No.	3. Recipient's Catalog No.
NASA TM-89120		

4. Title and Subtitle	5. Report Date
UNSTEADY TRANSONIC FLOW CALCULATIONS FOR REALISTIC AIRCRAFT CONFIGURATIONS	March 1987
	6. Performing Organization Code: 505-63-21-01
7. Author(s): John T. Batina, David A. Seidel, Samuel R. Bland, and Robert M. Bennett	8. Performing Organization Report No.
9. Performing Organization Name and Address: NASA Langley Research Center, Hampton, Virginia 23665-5225	10. Work Unit No.
	11. Contract or Grant No.
12. Sponsoring Agency Name and Address: National Aeronautics and Space Administration, Washington, DC 20546	13. Type of Report and Period Covered: Technical Memorandum
	14. Sponsoring Agency Code

15. Supplementary Notes

This paper will be presented at the AIAA/ASME/ASCE/AHS 28th Structures, Structural Dynamics and Materials Conference, Monterey, CA, April 6-8, 1987, as AIAA Paper No. 87-0850.

16. Abstract

A transonic unsteady aerodynamic and aeroelasticity code has been developed for application to realistic aircraft configurations. The new code is called CAP-TSD which is an acronym for Computational Aeroelasticity Program - Transonic Small Disturbance. The CAP-TSD code uses a time-accurate approximate factorization (AF) algorithm for solution of the unsteady transonic small-disturbance equation. The AF algorithm is very efficient for solution of steady and unsteady transonic flow problems. It can provide accurate solutions in only several hundred time steps yielding a significant computational cost savings when compared to alternative methods. The new code can treat complete aircraft geometries with multiple lifting surfaces and bodies including canard, wing, tail, control surfaces, launchers, pylons, fuselage, stores, and nacelles. Applications are presented for a series of five configurations of increasing complexity to demonstrate the wide range of geometrical applicability of CAP-TSD. These results are in good agreement with available experimental steady and unsteady pressure data. Calculations for the General Dynamics one-ninth scale F-16C aircraft model are presented to demonstrate application to a realistic configuration. Unsteady results for the entire F-16C aircraft undergoing a rigid pitching motion illustrated the capability required to perform transonic unsteady aerodynamic and aeroelastic analyses for such configurations.

17. Key Words (Suggested by Authors(s))	18. Distribution Statement
Transonic Unsteady Aerodynamics Aeroelasticity Flutter	Unclassified - Unlimited Subject Category 02

19. Security Classif.(of this report)	20. Security Classif.(of this page)	21. No. of Pages	22. Price
Unclassified	Unclassified	20	A02

For sale by the National Technical Information Service, Springfield, Virginia 22161